

3D-Printed Hydraulic Fluidic Logic Circuitry for Soft Robots

Yuxin Lin,¹ Xinyi Zhou,¹ Wenhan Cao^{1,2*}

¹School of Information Science and Technology, ShanghaiTech University, Shanghai 201210, China

²Shanghai Engineering Research Center of Energy Efficient and Custom AI IC, Shanghai 201210, China

*Correspondence: whcao@shanghaitech.edu.cn

Abstract

Fluidic logic circuitry analogous to its electric counterpart could potentially provide soft robots with machine intelligence due to its supreme adaptability, dexterity, and seamless compatibility using state-of-the-art additive manufacturing processes. However, conventional microfluidic channel based circuitry suffers from limited driving force, while macroscopic pneumatic logic lacks timely responsivity and desirable accuracy. Producing heavy duty, highly responsive and integrated fluidic soft robotic circuitry for control and actuation purposes for biomedical applications has yet to be accomplished in a hydraulic manner. Here, we present a 3D printed hydraulic fluidic half-adder system, composing of three basic hydraulic fluidic logic building blocks: AND, OR, and NOT gates. Furthermore, a hydraulic soft robotic half-adder system is implemented using an XOR operation and modified dual NOT gate system based on an electrical oscillator structure. This half-adder system possesses binary arithmetic capability as a key component of arithmetic logic unit in modern computers. With slight modifications, it can realize the control over three different directions of deformation of a three degree-of-freedom soft actuation mechanism solely by changing the states of the two fluidic inputs. This hydraulic fluidic system utilizing a small number of inputs to control multiple distinct outputs, can alter the internal state of the circuit solely based on external inputs, holding significant promises for the development of microfluidics, fluidic logic, and intricate internal systems of untethered soft robots with machine intelligence.

Introduction

Soft robotics has emerged as a promising avenue for the development of adaptable, bio-inspired robotic systems. Unlike their rigid counterparts, soft robots exhibit remarkable compliance and dexterity, making them well-suited for applications ranging from surgical devices [1-4] to search-and-rescue missions [5, 6]. At the heart of this emerging technology lies the ingenious concept of fluidic logic, which draws inspiration from the complex, yet highly efficient, hydraulic systems found in nature, such as the muscular hydrostats of cephalopods [7, 8] and the hydrostatic skeletons of worms for propulsion [9, 10]. One of the groundbreaking innovations in soft robotics is the integration of fluidic logic, a control mechanism that harnesses the flow of fluids, typically air or liquids, to control the movement and deformation of soft robotic structures in analogous to electric circuits. As an alternative to traditional electronic systems, fluidic actuation is a widely used propulsion technique in soft robotics. Soft robots primarily consist of materials that demonstrate significant compliance under normal loading conditions [11]. When the fluid volume inside the soft robot expands or contracts, the associated actuator

undergoes deformation due to the increased pressure. These deformations can be effectively utilized to perform gripping [12-14] and compressive [15] actions resembling claw-like structures. Further, by coordinating the deformation of multiple actuators, soft robots can also achieve locomotion capabilities [16-18].

Typically, rigid robots have to rely on electronic circuitry and connection wiring for control and actuation, offering precision and predictability in their movements. However, these systems often lack the adaptability and robustness required to navigate unstructured environments. Thus, reducing the strong reliance on external tethering connections and integrating essential components within the structure of the soft robotic systems would greatly enhance their utility and versatility [19]. This necessitates the specialized design of the fluidic system within soft robots mimicking the biomechanical principles observed in nature. An effective approach to address external constraints is the implementation of an oscillator as a control mechanism, generating alternating outputs. By employing an oscillator, a single input signal can be processed to concurrently control multiple channels [20-22]. Oscillator input could derive from chemical reaction [23, 24], external gas container [25] or micropumps [26]. These connected actuators react sequentially to the oscillator alternating outputs, resulting in a change in the system's posture or gait. These robots can potentially transform robotics industries by enabling safer human-robot interactions and enhancing the agility of autonomous machines.

Despite the potential benefits of soft robotic fluidic logic, the implementation of fluidic logic in soft robots poses significant challenges. First, developing highly responsive and efficient fluidic circuits using conventional pneumatic actuation mechanism at centimeter scale remains a significant obstacle. Furthermore, ensuring precise control and feedback mechanisms in fluidic logic-based soft robots is challenging due to the highly compressible nature of pneumatic fluid. In addition, the gas-liquid mixture system exhibits unsatisfying uniformity, and the presence of bubbles within the liquid can cause disturbances in pressure, thereby affecting the stability of the system. This greatly hampers the responsiveness and precision of the soft robot. The inherent compliance and deformability of these robots also introduce nonlinearities, making control and modeling more intricate. Achieving consistent and repeatable behaviors in dynamic and unstructured environments demands innovative solutions. Additionally, addressing the heavy-duty mechanical tasks such as wearable exoskeleton for rehabilitation and surgical robotic actuation operations would require substantial driving force for the actuators, which makes hydraulic sources way more preferable over pneumatic ones.

To meet these intricate requirements, soft robots need to develop advanced functionalities, leading to increased complexity in their control systems. In addition to oscillators, the incorporation of microfluidics and fluidic logic technologies becomes crucial. The typical utilization of microfluidic chips offer significant advantages by enabling complex fluid operations with minimal input, thereby enhancing the processing capacity of the fluidic network [27]. By adjusting inputs, microfluidic chip facilitates output control without the requirement of external devices for intermediate steps, eliminating the need for additional processing components in the system [28].

With the advances in processing technologies, various fabrication methods and components have been employed in microfluidic systems [29], including soft lithography [30], molding [31, 32] and micro 3D printing [32-36]. Application of these technologies facilitates the manufacturing of intricate logic, and thereby results in enhanced

performance and functionality. In 2003, a three-layer valve design was introduced, incorporating non-thermal device bonding [37]. Membrane valves are widely used in microfluidic systems, where an elastic membrane deforms under pneumatic actuation to control the channel state [38].

Designing the valve system in a manner that allows smaller control inputs to effectively regulate larger outputs in analogous to electronic transistors greatly expands the application possibilities of the valve itself. This can be achieved by implanting rigid discs within the deformable membrane, enabling the control pressure to act over the entire bottom side of the disc layer, while the source pressure acts only over the orifice area when the valve is closed [39]. Leveraging unequal area differences or ensuring that the input force arm is shorter than the control force arm can achieve the same effect [40].

These principles enable the use of low pressure to control high pressure.

Currently, there is a growing emphasis on the development of fluidic devices that can perform complex sample treatment while also implementing Boolean functions [41]. Analogies can be drawn between water flow and electric current. Similar to how electric current is generated by voltage, water pressure drives water flow. Both electric current and water flow experience resistance during their flow, which can be quantified using Ohm's law and its fluidic analogy, Poiseuille's law, respectively. The flow rates of electric current and liquid can be utilized to measure their flow characteristics, and the properties of the circuit enable the determination of voltage and fluid pressure variations within the system [42]. In theory, if designed appropriately, microfluidic systems can achieve certain functions of microelectronic systems through fluidic circuits and microfluidic devices typically made with polydimethylsiloxane (PDMS). Unfortunately, while extensively studied, mostly microfluidic logic circuitry based on small deformation of PDMS membrane and transformation of small amount of liquid fluid, rendering it unsuitable for driving large-scale end-effector mechanisms such as exoskeletons and grippers for rehabilitation purposes.

Fluidic logic simplifies the construction and operation of complex electronic devices, reducing the need for off-chip controllers [43]. Tension-based passive pumping and fluidic resistance can create microfluidic analogies to electronic circuit components [44, 45] with special fluid characteristics [35, 46]. The on-off control of valves in the control channel can serve as a signal [31, 47], and fluid flow through specific locations can also function as a signal [48]. Corresponding gates can be designed based on MOSFETs, mimicking the behavior of transistor circuits [49, 50]. In addition to basic logic gates, demultiplexers have been developed to efficiently control multiple outputs with fewer inputs in a microfluidic manner [51]. Furthermore, fluidic circuits that perform addition operations have been proposed, offering branching effects and output control capabilities [45, 52-54]. While current study on microfluidic channel based fluidic logic have shown promises in their potential applications in integration with soft robots, achieving logic gate functions poses significant challenges and requirement for high flow rate at a certain level for centimeter scale actuation and biomedical purposes has yet to be accomplished. Thus, understanding the scaling effect of fluidic circuitry and effectively utilizing different components are key to building fluidic logic at such a larger scale.

Fluidic analog circuits, activated by continuous input, have been utilized in the control of soft robots to autonomously perform predefined tasks, eliminating the need for manual intervention [23, 25, 55]. The principles of complementary metal oxide semiconductor

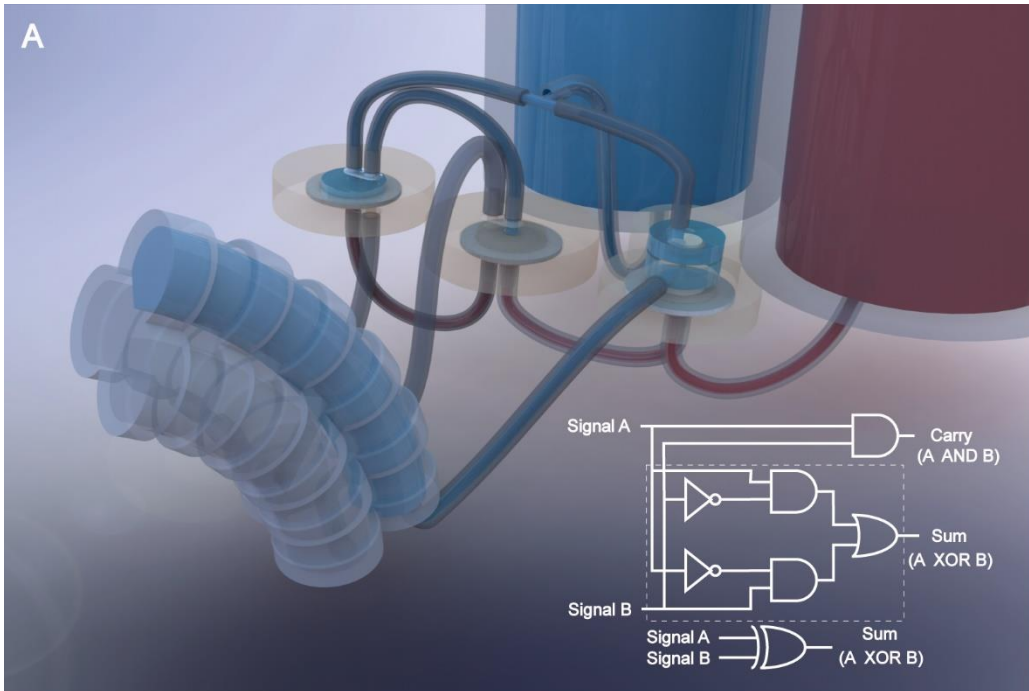
(CMOS) circuits have also been applied to control soft robots, enabling them to exhibit inchworm-like movement [50] and arm-bending capabilities [56] through pneumatic actuation. D-type latch and shift register is designed to drive actuator combined with demultiplexer [47]. However, as the circuit complexity and number of valves increase, friction losses along the circuit also intensify. This challenge can be mitigated by increasing the number of inputs in the intermediate process or elevating the initial input pressure. Nonetheless, it is often observed that the functionalities of these intermediate channels are not fully utilized, and adding inputs could introduce more constraints. Due to its incompressible nature, hydraulic fluidic logic circuitry becomes ideal candidates for tackling these issues for achieving heavy duty and highly responsive actuation, as well as seamless integration with soft robots, at a centimeter scale.

When a circuit becomes structurally complex due to functional requirements, the introduction of arithmetic logic can simplify the circuit structure, reducing delay and the number of circuit gates used. The half-adder is a vital integral component of arithmetic logic unit, and implementing a fluidic half-adder serves as the foundation for fluidic arithmetic logic. In addition to performing logical operations, a fluidic half-adder must ensure non-interference between different channels, maintain a desired output pressure magnitude, and employ channel multiplexing to minimize the use of logic gates and reduce system complexity. Therefore, designing an efficient fluidic half-adder presents a significant challenge.

In this Article, we first develop hydraulic fluidic building blocks of basic OR, NOT, and AND logic gates using 3D printing techniques and other readily available polymeric materials. Our team then focus on logical operations and introduce a XOR fluidic logic gate consisting of dual NOT valves. Following the principles of adder circuits, we design and fabricate two variations of half-adder circuits, which are core components of arithmetic logic unit in a modern computer. These circuits effectively utilize the input and output channels of each valve, enabling purely hydraulic logical computing capabilities within the fluidic system. In addition, we enhanced the two half-adder fluidic circuits to enable the hydraulic logic control of a three degree-of-freedom (DOF) soft robotic actuator. The integration of hydraulic fluidic logic into soft robotics holds great promises for the development of adaptable, responsive, bio-inspired, and wearable intelligent soft machines.

Results

Basic hydraulic logic gate as building blocks



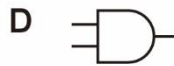
Input 1	Input 2	Output
0	0	0
1	0	1
0	1	1
1	1	1

OR



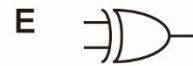
Input	Output
0	1
1	0

NOT



Input 1	Input 2	Output
0	0	0
1	0	0
0	1	0
1	1	1

AND



Input 1	Input 2	Output
0	0	0
1	0	1
0	1	1
1	1	0

XOR

Fig .1. Schematic of hydraulic actuation using fluid half adder built upon basic logic gates. (A) Using modified hydraulic fluid half to control soft robot. The truth tables of (B) OR, (C) NOT, (D) AND, and (E) XOR logic gates.

Complex logical operations are combinations of basic logical operations, including disjunction (OR), negation (NOT), and conjunction (AND) gates, each corresponding to a specific truth table in Fig. 1. To achieve diverse fluidic logic, it is essential to design fundamental fluidic components capable of performing these three basic logical operations. In fluidic logic circuits, "0" in the truth table commonly represents the absence of fluid flow at a certain pressure, while "1" represents the presence of fluid flow at a certain pressure. Therefore, three basic valve structures and flow configurations are designed separately to meet the input-output requirements for each logical operation.

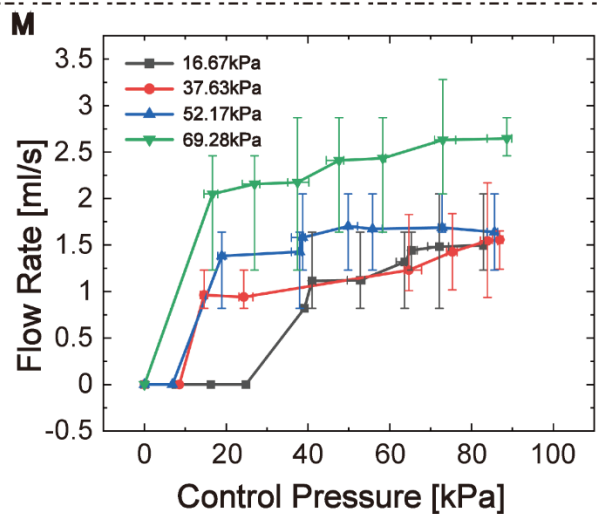
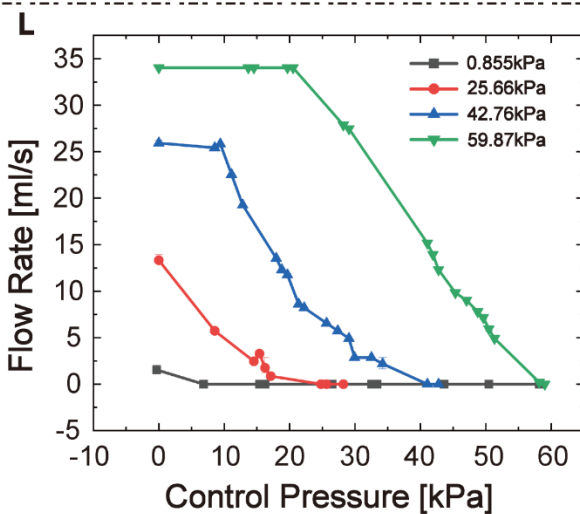
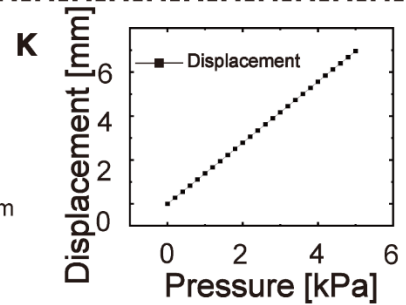
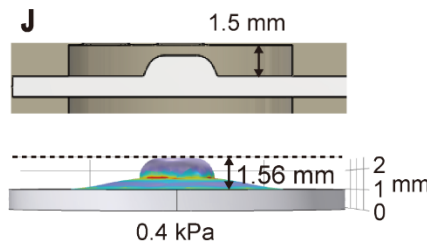
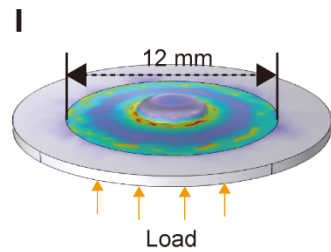
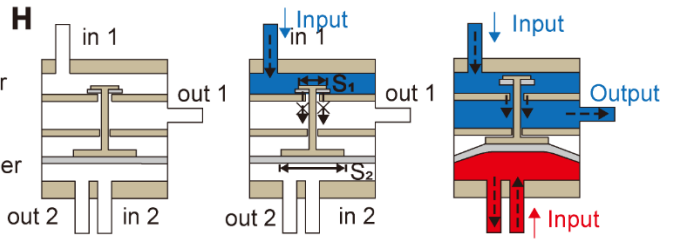
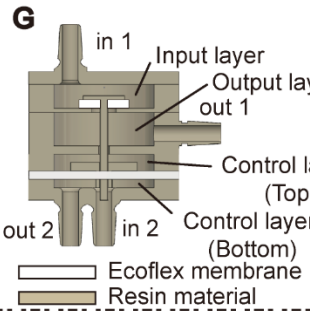
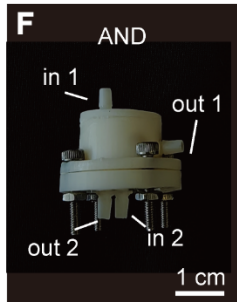
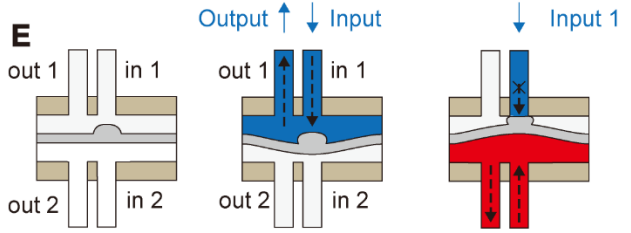
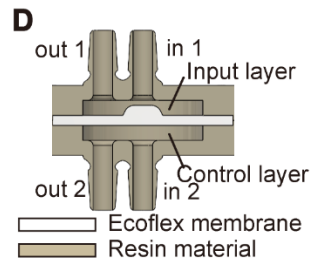
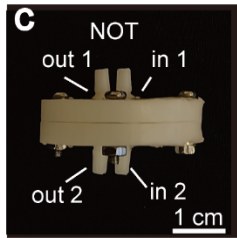
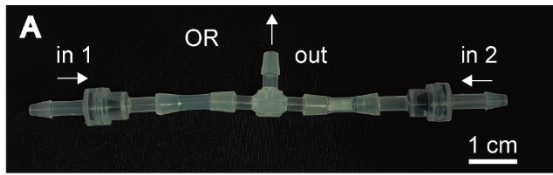


Fig. 2. Geometry and performance characterization of basic logic gates. (A) The OR gate is composed of two check valves using a T-shaped junction. (B) Schematic illustration of OR gate. (C) Picture of 3D printed NOT gate device. (D) Cross-section of NOT gate. (E) Operating principle of NOT gate. (F) Picture of AND gate. (G) Cross-section of AND gate. (H) Operating principle of AND gate. (I) Finite element analysis simulation of load distribution in membrane. (J) Displacement of the top of the membrane under a load of 0.4 kPa. (K) Relationship between displacement of the top of membrane and load. (L) Flow rate-control pressure characteristic curve for NOT gate under constant input pressure conditions. (M) Flow rate-control pressure characteristic curve for AND gate under constant input pressure conditions.

To implement the disjunction (OR) operation, we utilize a T-shaped junction and two check valves in a specific configuration, as shown in Fig. 2A. The T-shaped junction guarantees that when one interface receives a continuous liquid input, the liquid will flow towards the remaining two ports. In our design, the central channel of T-shaped junction serves as the output pathway, while the left and right channels act as the input pathways. To ensure the fluid flow from "input" to "output" and prevent undesired scenarios like "input" to "input" or backflow, a unidirectional check valve is incorporated at each input port. This arrangement establishes a unidirectional flow path within the device, aligning with the intended logic operation Fig. 1B.

To implement the negation (NOT) operation, we design a valve shown in Fig. 2C, with the yellow region fabricated by stereolithography 3D printing. The valve consists of a control cavity and an input cavity (Fig. 2D), interconnected with external pipelines through the input channel and output channel. Within the valve, an elastic silicone membrane made of Ecoflex 00-30 is positioned. The membrane is asymmetric, featuring a centrally located cylindrical protrusion on its upper side that can connect to the input cavity. The specific membrane design aims to reduce the distance between the membrane and the input channel, so that less deformation is required for the closure of the input channel compared to the one of control layer. The operational principle of the valve is as follows: when the pressure in the control cavity reaches a specific threshold, the elastic membrane expands and deforms, obstructing the input channel and halting the fluid flow. The relationship between the average input pressure and control pressure at the critical channel closure position is depicted in Fig. 2E. The input-output relationship of this valve aligns with the truth table of NOT gate presented in Fig. 1C.

To implement the conjunction (AND) operation, we design a valve as shown in Fig. 2F. The valve consists of four cavities (Fig. 2G): Cavity 1 and 2 form the input cavity, with Cavity 1 connected to the input channel and Cavity 2 connected to the output channel. Cavity 3 and 4 make up the control cavity, with Cavity 4 interconnected with the control channel. A disc-pole-disc structure runs through the cavities, while a 1 mm-thick Ecoflex elastic membrane is attached to the lower side of Cavity 1 to act as a carrier ring during compression. When pressuring the control cavity, the disc-pole-disc structure is risen and the channel in input cavity is opened, causing fluid predominantly exiting through output channel. While depressurizing the control cavity causes the disc-pole-disc structure to descend, closing the channel and blocking the outflow. Force summation occurs over the rigid discs-pole-disc[39]. When the channel in input cavity is in the closed state, due to the unequal pressured areas between the upper and lower discs, the disc-pole-disc can

still rise even though the control pressure is smaller than the input pressure, achieving the purpose of using a lower pressure to control fluid with a higher pressure (Fig. 2H).

Besides realizing the truth table of AND gate (Fig. 1D), this configuration can be conceptually likened to a transistor and a threshold controller.

We conducted simulations to investigate the deformation effect of the designed membrane under different load, aiming to verify its capability to close the channel. The load was applied to a 12 mm diameter region at the middle of the membrane, as illustrated in

Fig. 2I. As depicted in Fig. 2J, when the load reached 0.4 kPa, the distance from the top of the membrane to the membrane plane measured 1.56 mm. This distance exceeded the separation between the membrane plane and the channel, demonstrating that the membrane deformation was adequate to close the channel under a small load.

Additionally, a thorough examination of the displacement of the top of the membrane in relation to the load size was conducted. The simulation results, shown in Fig. 2K, revealed a linear relationship between the two variables. Thus, precise control of the membrane's top-end displacement can be achieved by adjusting the load size.

In order to test the functionality with and without gates, we designed experiments to measure the relationship between the output flow rate and the control pressure at different input pressures. The results of with and without gates are shown in Fig. 2L, Fig. 2M. It can be seen from the figures that as the control pressure increases, the output flow rate increases and decreases with gate and non-gate respectively, which is in accordance with the expected results.

Implementation of hydraulic XOR system

As for the XOR operation, the XOR device is constructed by two NOT gates, as shown in Fig. 3A. Historically, this particular architecture has been employed as an oscillator in certain devices. As the membrane is designed to be asymmetric, closing the inlet of input cavity is easier than closing the inlet of control cavity. Within one NOT gate, when fluid input is introduced, increasing pressure in the control cavity of NOT gate quickly leads the channel closed, preventing fluid from flowing out through the outlet. Taking the two connected NOT gates into consideration, the input fluid flow state of one NOT gate can influence the channel switch state of this NOT gate, at the same time acts as the control signal of the other NOT gate. In this way, if fluid is introduced into one NOT gate as source and the channel within the other NOT gate remains open due to no fluid input, fluid will eventually flow out of outlet 2, representing Output "1" in the truth table. Fluid flowing out of outlet 2 could be logically interpreted as $a \cap \neg b$ or $b \cap \neg a$, as shown in Fig. 3B. Using an OR gate to connect the outlet 2 of these two NOT gates like Fig. 3C, the output of OR gate could be interpreted as $(a \cap \neg b) \cup (b \cap \neg a)$, conforming the XOR operation corresponding to Fig. 1E.

As the output is a constant 0 when no fluid is introduced, the device naturally suffices the situation where the truth table inputs are all 0. When there are 2 inputs, as shown in Fig. 3C, the interpretation of outlet of OR gate could be simplified as $\neg b \cup \neg a$. By using another NOT gate to process this signal, we can achieve the performance of AND gate, which could be used to take the place of AND gate as shown in Fig. 3D. Figs. 3E-H show the output of different input states.

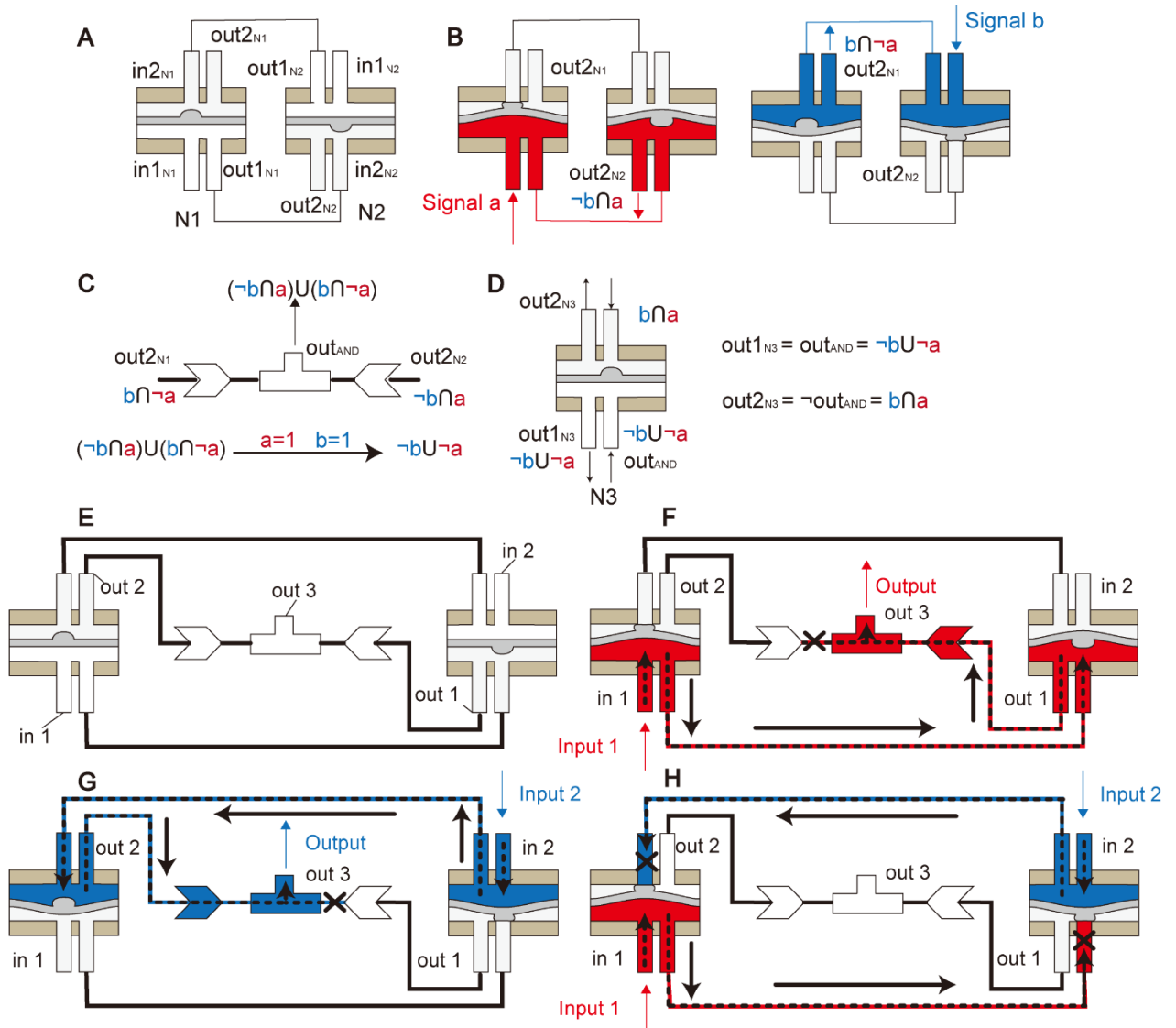


Fig. 3. Implementing XOR and AND operations through gate combinations. (A) Schematic illustration of dual NOT gates system. (B) Logic interpretation of the output channel of the dual NOT gate system. (C) Implementing XOR operation by connecting two output channels of dual NOT gate systems through an OR gate. (D) Implementing AND operation by setting the output of XOR system as the input of a NOT gate. (E) Schematic illustration of XOR system. (F) (G) (H) are the modification and output states of XOR gate system in response to single input and double inputs.

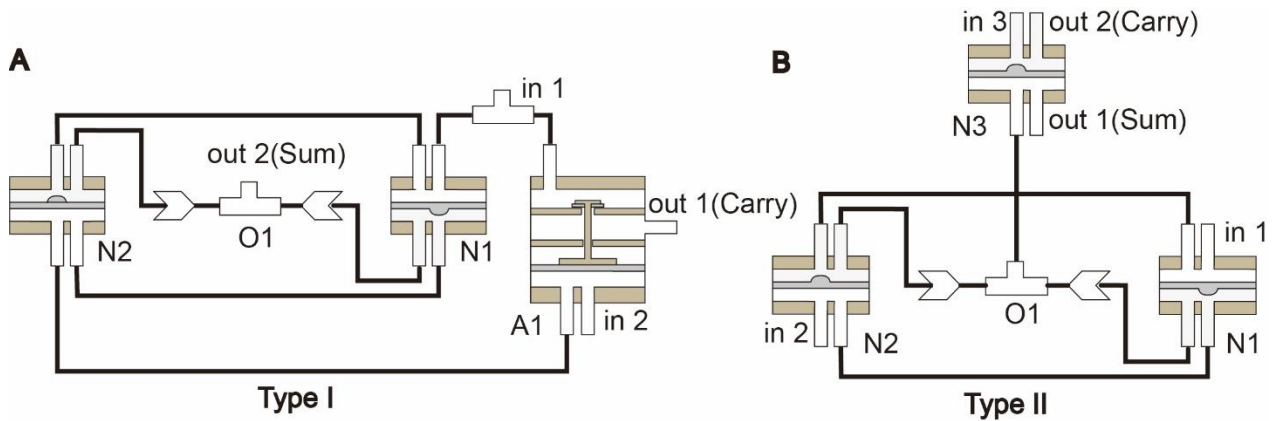


Fig. 4. Configurations of two alternative types of half adders. (A) Half adder (type I) composed of two NOT gates, one AND gate, and one OR gate. (B) Half adder (type II) composed of three NOT gates and one OR gate.

Half adder system and performance characterization

Building upon the existing apparatus for realizing the fundamental logical operations of fluidic AND, OR, and NOT gates, we devise two distinct fluidic circuits that embody the truth table mapping the relationship of a half adder.

The type I, as illustrated in Fig. 4A, bears the structural resemblance to a conventional electric half adder, comprising two constituent sections: an AND gate and an XOR gate. The device incorporates two input channels and two output channels, which respectively correspond to the Sum and Carry bits of the half adder.

When fluid only flows into inlet 1, as there is no control pressure in AND gate, the output of AND gate serving as Carry bit is blocked. In this condition, fluid will flow through the XOR gate and eventually flows out of the outlet serving as Sum bit (Fig. 5A). However, if fluid is only introduced through inlet 2, as there is no direct connection between inlet 2 and outlet within the AND gate, the value of Carry bit is naturally “0” and fluid will flow out of the outlet representing Sum bit (Fig. 5D). Moreover, with inlet 1 and 2 both introduced with fluid inputs, the XOR system operates and the channel within AND gate is opened, bringing fluid flowing through the outlet of AND gate and the Carry bit being “1” (Fig. 5G). By controlling the input signal we can produce responses that match the inputs “10” (Fig. 5C), “01” (Fig. 5F) and “11” (Fig. 5I) of the half adder. The observed responses are as expected and the waveform is stable.

The type II entails the integration of an XOR gate and a NOT gate as illustrated in Fig. 4B, where the two outlets of NOT gate serve as Sum and Carry bits respectively.

Notably, due to the additional input of NOT gate required for carry propagation, this configuration exhibits characteristics akin to a full adder; nevertheless, the truth table properties exhibited by the device remain consistent with those of a half adder.

When fluid flows into inlet 1, the XOR gate firstly operates and delivers its output fluid to the NOT gate. As there is no control pressure in NOT gate, fluid will only flow out of the outlet serving as Sum bit, leading Sum bit to be “1” and Carry bit to be “0” (Fig. 6A). This situation is also applicable to fluid input through inlet 2 (Fig. 6D). Additionally, when fluid flows into both inlet 1, 2 and 3, XOR gate transfers no output fluid to AND gate, leading the membrane to bend towards the lower cavity. Fluid flowing from source will flow out through the outlet serving as Carry bit (Fig. 6G). We obtained results with

signal inputs of "10" (Fig. 6C), "01" (Fig. 6F) and "11" (Fig. 6I) which also satisfy the truth table of the half adder.

Comparing Fig. 5I and Fig. 6I, we observe significant differences in the carry outputs of the two half adders. This discrepancy is attributed to a decrease in pressure caused by the flow of liquid through the orifice structure within the AND gate [57], as illustrated in Fig. S2.

Control of soft actuator using hydraulic signals

We selectively adjust these two different configurations of half adders, so that the deformation of a soft robotic tentacle in three distinct directions can be controlled solely through the fluid input status of the half adder. For the soft robotic tentacle, by introducing fluid into one of the three cavities, the internal pressure increases, causing expansion and deformation of the cavity into which the fluid is introduced. Typically, such hydraulic systems enjoy advantages over pneumatic ones in terms of actuation capabilities (Fig. S1).

Regarding the first scheme, the OR gate is dismantled, thereby allowing the outlets of the two NOT gates to be respectively connected to two separate cavities of the tentacle, while the outlet of the AND gate is connected to the remaining cavity, as shown in Fig. 7A. The methods to separately control the deformation of three cavities are depicted in Fig. 7B, Fig. 7C, and Fig. 7D. Similar to the situation discussed in the XOR gate chapter, one NOT gate can have a fluid output when the other NOT gate has a fluid input. So, when fluid is introduced into inlet 1 or 2, a corresponding connected cavity will deform and cause the tentacle to bend, as shown in Fig. 7B and Fig. 7C. When both inlet 1 and 2 have fluid inflow, the output channel in NOT gates are both blocked and the disc-pole-disc structure in AND gate is lifted up, opening the upper cavity, so that the corresponding tentacle cavity is filled with fluid and bends to the ground (Fig. 7D).

For the second scheme, our proposed solution entails introducing an additional conduit before each unidirectional check valve to establish connections with two distinct cavities, as shown in Fig. 7E. Similarly, if inlet 1 or 2 has fluid inflow, regardless of the status of pressure source, the tentacle will correspondingly bend due to pressure increase within cavities (Fig. 7F and Fig. 7G). Fluid from pressure source have no interference, as the output channel in the NOT gate is blocked by the output fluid flowing from the XOR gate. However, under the condition that fluid is introduced into all the inlets, there will be no fluid flowing out of XOR gate, allowing the output channel within NOT gate in open state. So, fluid provided by pressure source can flow out to the cavity and make the tentacle bend (Fig. 7H).

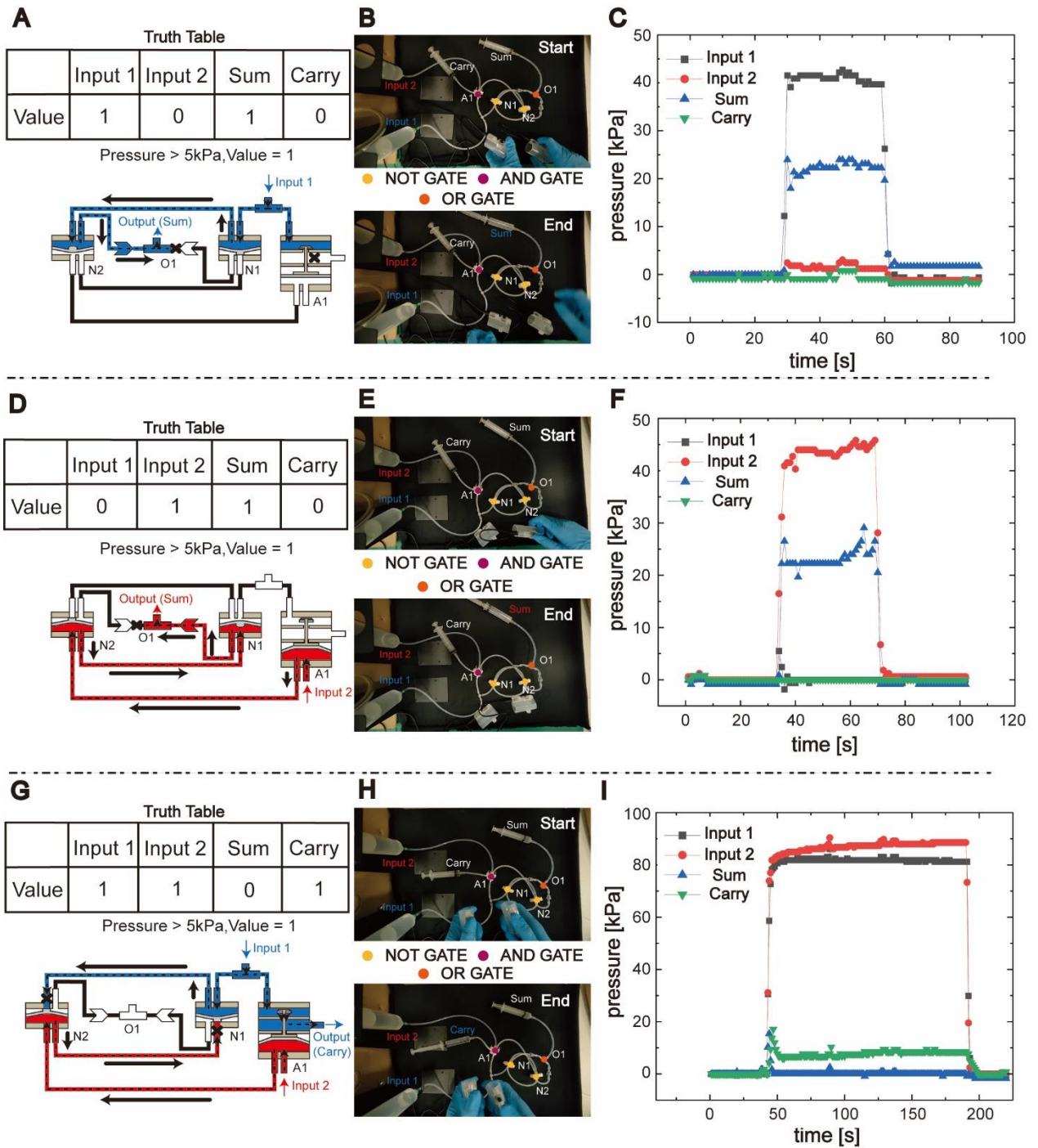


Fig. 5. Results of half adder (type I) performance in response to two inputs. (top row) (A) Given a “10” input using experimental setup (B), Sum exhibits high pressure while Carry remains low output (C). (middle row) (D) Similarly, given a “01” input using experimental setup (E), Sum also exhibits high pressure while Carry remains low output (F). (bottom row) (G) Given “11” or both high inputs, using experimental setup (H), Carry exhibits high pressure while Sum remains low output (I), sufficing the truth table of typical half adders.

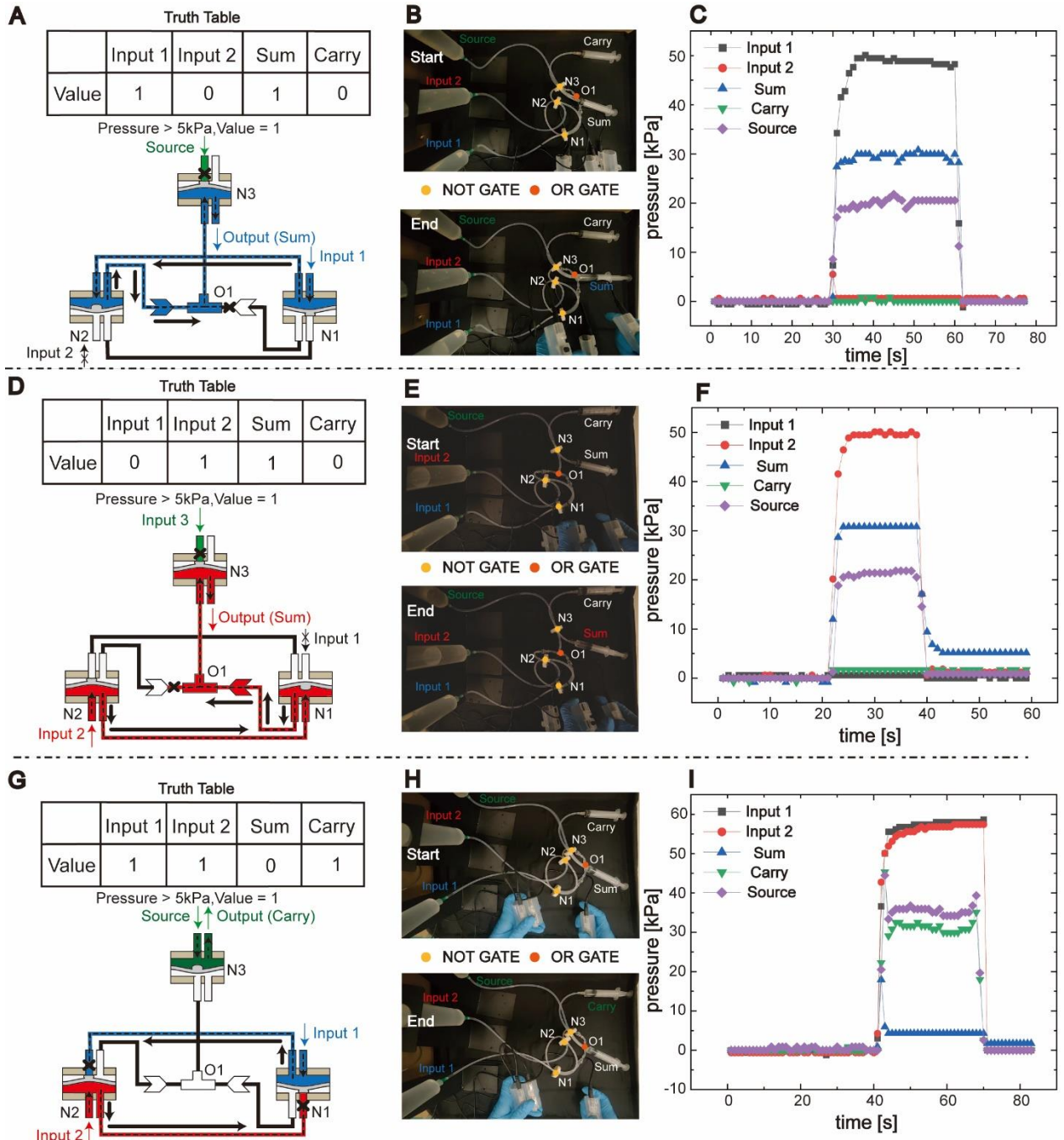


Fig. 6. Results of half adder (type II) with enhanced performance in response to two inputs using an additional pressure source. (top row) (A) Given a “10” input using experimental setup (B), Sum exhibits higher hydraulic pressure than type I case while Carry remains low output (C). (middle row) (D) Similarly, given a “01” input using experimental setup (E), Sum also exhibits high pressure while Carry remains low output (F). (bottom row) (G) Given “11” or both high inputs, using experimental setup (H), Carry exhibits high pressure while Sum remains low output (I), improving both Sum and Carry hydraulic pressure with the help of the additional pressure source, compared to type I half adder.

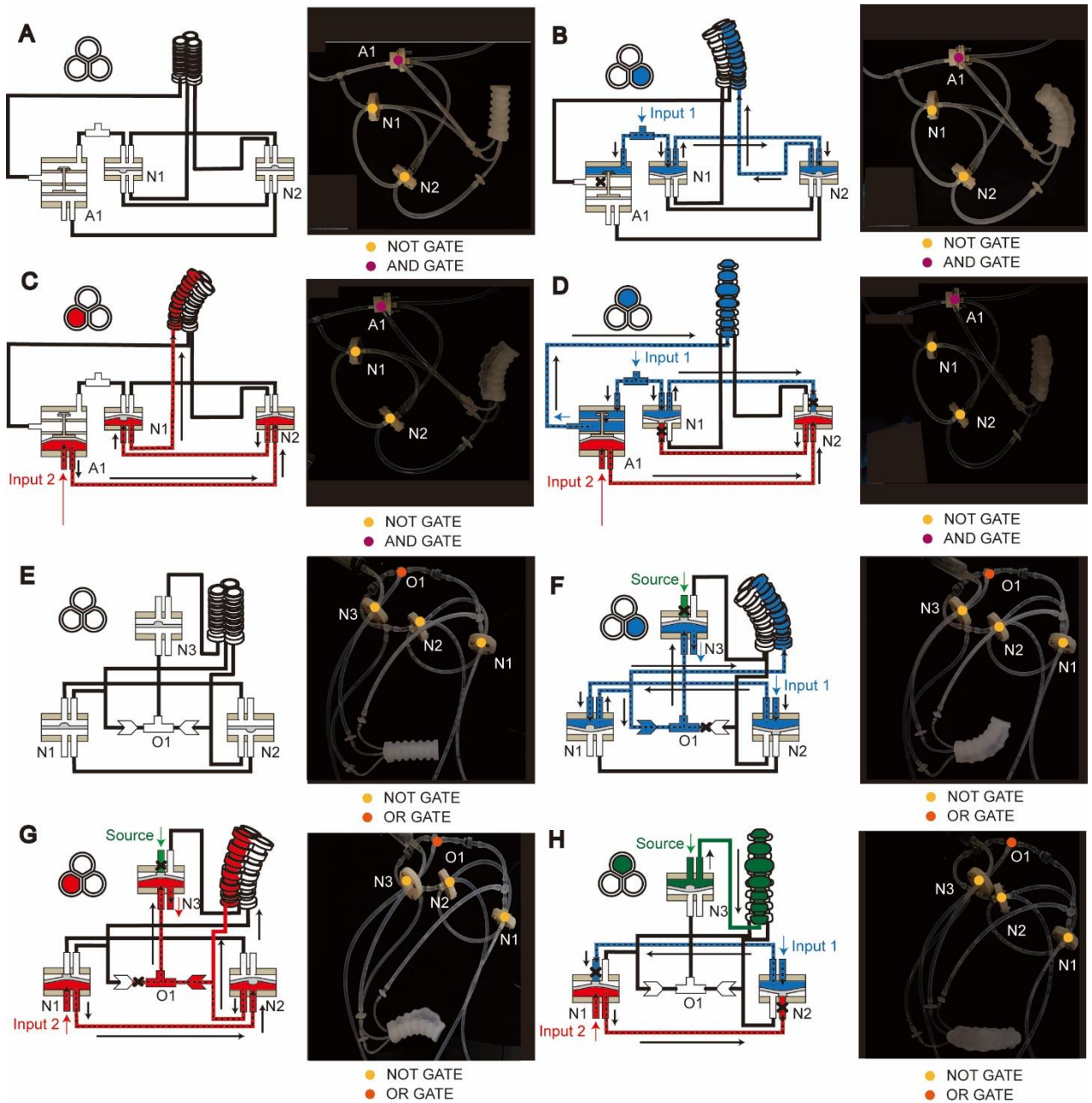


Fig. 7. Controlling a 3-DOF soft robotic actuation in three directions using modified half adder (type I and II). (A to D) Using half adder (type I) and (E to H) Using half adder (type II). (B) and (F) Using Input 1 to control the bending of left cavity. (C) and (G) Using Input 2 to control the bending of right cavity. (D) Using Input 1 and Input 2 to control the bending of middle cavity. (H) Using Input 1, Input 2 and an additional pressure source to control the bending of middle cavity.

Discussion

In this Article, we have undertaken a selection and design process to engineer structures capable of performing the fundamental hydraulic fluidic logic operations of AND, OR,

and NOT. Through their combination and cascading, we have realized a fluidic circuit for the implementation of a half adder, a crucial component in digital computation. Notably, by selectively adjusting channels within the device, we have achieved the control of a soft robotic tentacle's deformation in three distinct directions solely by manipulating the states of its two input variables. The devised apparatus holds significant research significance on multiple fronts. Firstly, it fulfills the requirement of achieving multiple output control through the utilization of a limited number of inputs—a crucial aspect in the field of logic design. Secondly, it enables the control of high-pressure circuits through the utilization of low-pressure inputs, presenting an advantageous capability for effective and efficient control in fluidic systems. Additionally, the device retains the inherent capacity to perform logical operations, thereby facilitating the implementation of complex decision-making processes within the system. Moreover, the outputs of the device can be utilized to drive the actuators of the soft robotic end effector, enabling practical applications in the field of soft robotics. Furthermore, the device exhibits an expandable design space, allowing for the incorporation of various interconnected units to construct more intricate circuitry. This feature offers the potential to realize sophisticated control schemes, thus enabling the realization of complex modal motions in robots driven by simple inputs. Notably, the entire control process is executed purely by fluidic means, obviating the need for external electronic circuits. This novel characteristic provides a promising design paradigm for the internal systems of untethered soft robots, offering enhanced versatility and maneuverability through fluidic logic.

Materials and Methods

FEM analysis of membrane

The deformation simulation of membrane under different pressure was conducted in COMSOL Multiphysics using solid mechanics module. In addition to applying loads to the membrane center with a diameter of 12 mm, we have added fixed constraints in the diameter range of 12 mm to 18 mm as this region is sticking to the rigid body.

Basic hydraulic logic gates fabrication

Based on the materials used and the different structures of the valves, we have developed different assembly schemes for the three valve designs. The OR gate is assembled by connecting a T-shaped junction and two check valves. They are commonly used components for pipe connections, and their assembly is straightforward. The use of silicone tubing for the connections results in minimal loss along the pipeline due to its short length. For the NOT gate and AND gate, we employ a facile layered design. After assembling the layers, glue is used for bonding, and four screws and bolts are used for providing additional reinforcement and robustness (details shown in Fig. S3 and Fig. S4). The rigid shells of the NOR gate and XOR gate are produced using a UV curing printer (HALOT-RAY, CREALITY, China) with UV curable resin (3D Printer UV Curable Resin Standard Resin Plus, White, CREALITY, China) as the printing material. The elastic membrane is made by pouring and molding a mixture of silicone (Ecoflex 00-30, Smooth-On, Inc., USA) part A and B in a ratio of 2 to 3.

Experiment of AND gate and NOT gate flow rate-control pressure testing

Considering the possibility of applying the theory of COMS circuits to fluid circuits, we conducted tests on the flow-control pressure characteristics of the NOR gate and XOR gate. The tests required the use of a pressure sensor (XGZP6847A, 0-700 kPa, CFSensor, China) and a flow meter (YRS-SFR, 1-200 ml/min, Shanghai Urisi Instrument Co., LTD, China). Both the sensor and flow meter were connected to the logic gates through silicone tubing within a 10 cm range. It should be noted that flow rates are often measured in standard measurement time units, typically minutes, using the rise and fall of pulse signals. We calibrated the flow meter using a syringe pump (LSP04-1A, Longer Pump, China). When the flow rate of the injection pump was set to 25 ml/min, the flow meter outputted 4 pulse signal changes per second. This corresponds to a flow rate of 0.41 ml/s per pulse. The sensor and flow meter were both connected to an Arduino board (Arduino UNO, ARDUINO, Italy), and the sampling frequency was set to 1 Hz. The wiring diagram of NOT gate and AND gate testing are showed in Fig. S5 and Fig. S6. Due to the performance of the flow meter itself and the influence of the sampling period, slight fluctuations in the pulse count may occur when the flow rate is low. Therefore, we took multiple measurements and averaged the results obtained from adjacent pressure measurements to reduce the impact. The results are shown in Fig. 1D and Fig. 1E.

Experiment of half adder type I and type II

Experimental device is shown in Fig. S7. We used three small dispensing machines (BXH-982A, Ben Xin He, China) as stable pressure sources for the experiment. The air pressure input of the dispensing machines was controlled by an electric inflator pump, and the output pressure was adjusted using the knobs on the control panel. The output channels were connected to the corresponding dispensing syringes, and the water pressure in the input system was controlled by changing the air pressure above the water surface. For this procedure, we used pressure sensors (XGZP6847A, 0-700 kPa, CFSensor, China) and (XGZP6847A, 0-500 kPa, CFSensor, China). The dispensing machines were controlled by an external button to toggle their working status. When the button was pressed, the dispensing machine started and pressurized the system. Releasing the button stopped the dispensing machine, and the system pressure dropped to 0 kPa. The dispensing machines were used to control the input channels of the half adder.

Experiment of 3-DOF soft actuation

We also conducted driving experiments on a three-degree-of-freedom soft robotic actuator using the dispensing machine as a pressure source. The soft robotic actuator was fabricated by pouring and molding silicone (Ecoflex 00-30, Smooth-On, Inc., USA) with a 1:1 base to crosslinker mixing ratio. We applied the same air pressure as in the half adder experiment to observe the performance of the soft robotic actuator.

References

1. Cianchetti, M., et al., *Biomedical applications of soft robotics*. Nature Reviews Materials, 2018. **3**(6): p. 143-153.
2. Zhu, J., et al., *Intelligent Soft Surgical Robots for Next-Generation Minimally Invasive Surgery*. Advanced Intelligent Systems, 2021. **3**(5).
3. Rogatinsky, J., et al., *A multifunctional soft robot for cardiac interventions*. Science Advances, 2023. **9**(43).
4. Tang, W., et al., *Self-protection soft fluidic robots with rapid large-area self-healing capabilities*. Nature Communications, 2023. **14**(1).

5. Hawkes, E.W., et al., *A soft robot that navigates its environment through growth*. Science Robotics, 2017. **2**(8).
6. Mintchev, S., et al., *A Soft Robot for Random Exploration of Terrestrial Environments*, in *2018 IEEE International Conference on Robotics and Automation (ICRA)*. 2018. p. 7492-7497.
7. Laschi, C., et al., *Soft Robot Arm Inspired by the Octopus*. Advanced Robotics, 2012. **26**(7): p. 709-727.
8. De Pascali, C., et al., *3D-printed biomimetic artificial muscles using soft actuators that contract and elongate*. Science Robotics, 2022. **7**(68).
9. Zhang, B., et al., *Worm-Like Soft Robot for Complicated Tubular Environments*. Soft Robotics, 2019. **6**(3): p. 399-413.
10. Niu, H., et al., *MagWorm: A Biomimetic Magnet Embedded Worm-Like Soft Robot*. Soft Robotics, 2021. **8**(5): p. 507-518.
11. Rus, D. and M.T. Tolley, *Design, fabrication and control of soft robots*. Nature, 2015. **521**(7553): p. 467-75.
12. Rothemund, P., et al., *A soft, bistable valve for autonomous control of soft actuators*. Science Robotics, 2018. **3**(16): p. eaar7986.
13. Zhai, Y., et al., *Desktop fabrication of monolithic soft robotic devices with embedded fluidic control circuits*. Science Robotics, 2023. **8**(79).
14. Jin, L., et al., *Ultrafast, Programmable, and Electronics-Free Soft Robots Enabled by Snapping Metacaps*. Advanced Intelligent Systems, 2023. **5**(6).
15. Song, S., et al., *Controllable load sharing for soft adhesive interfaces on three-dimensional surfaces*. Proc Natl Acad Sci U S A, 2017. **114**(22): p. E4344-E4353.
16. Shepherd, R.F., et al., *Multigait soft robot*. Proc Natl Acad Sci U S A, 2011. **108**(51): p. 20400-3.
17. Tang, Y., et al., *Switchable Adhesion Actuator for Amphibious Climbing Soft Robot*. Soft Robot, 2018. **5**(5): p. 592-600.
18. Robertson, M.A. and J. Paik, *New soft robots really suck: Vacuum-powered systems empower diverse capabilities*. Sci Robot, 2017. **2**(9).
19. Rich, S.I., R.J. Wood, and C. Majidi, *Untethered soft robotics*. Nature Electronics, 2018. **1**(2): p. 102-112.
20. Mosadegh, B., et al., *Integrated Elastomeric Components for Autonomous Regulation of Sequential and Oscillatory Flow Switching in Microfluidic Devices*. Nat Phys, 2010. **6**(6): p. 433-437.
21. Duncan, P.N., T.V. Nguyen, and E.E. Hui, *Pneumatic oscillator circuits for timing and control of integrated microfluidics*. Proc Natl Acad Sci U S A, 2013. **110**(45): p. 18104-9.
22. Kim, S.J., R. Yokokawa, and S. Takayama, *Microfluidic oscillators with widely tunable periods*. Lab Chip, 2013. **13**(8): p. 1644-8.
23. Wehner, M., et al., *An integrated design and fabrication strategy for entirely soft, autonomous robots*. Nature, 2016. **536**(7617): p. 451-5.
24. Hughes, J. and D. Rus, *Mechanically programmable, degradable & ingestible soft actuators*. in *2020 3rd IEEE International Conference on Soft Robotics (RoboSoft)*. 2020. IEEE.
25. Drotman, D., et al., *Electronics-free pneumatic circuits for controlling soft-legged robots*. Science Robotics, 2021. **6**(51): p. eaay2627.
26. Lee, W.-K., et al., *A buckling-sheet ring oscillator for electronics-free, multimodal locomotion*. Science Robotics, 2022. **7**(63): p. eabg5812.
27. Thorsen, T., S.J. Maerkl, and S.R. Quake, *Microfluidic large-scale integration*. Science, 2002. **298**(5593): p. 580-584.
28. Leslie, D.C., et al., *Frequency-specific flow control in microfluidic circuits with passive elastomeric features*. Nature Physics, 2009. **5**(3): p. 231-235.
29. Whitesides, G.M., *The origins and the future of microfluidics*. Nature, 2006. **442**(7101): p. 368-73.
30. Unger, M.A., et al., *Monolithic microfabricated valves and pumps by multilayer soft lithography*. Science, 2000. **288**(5463): p. 113-6.
31. Zhang, S., B. Kwak, and D. Floreano, *Design and manufacture of edible microfluidic logic gates*, in *2023 IEEE International Conference on Soft Robotics (RoboSoft)*. 2023. p. 1-7.
32. Glick, C.C., et al., *Rapid assembly of multilayer microfluidic structures via 3D-printed transfer molding and bonding*. Microsystems & Nanoengineering, 2016. **2**(1).

33. Rogers, C.I., et al., *3D printed microfluidic devices with integrated valves*. *Biomicrofluidics*, 2015. **9**(1): p. 016501.
34. Keating, S.J., et al., *3D Printed Multimaterial Microfluidic Valve*. *PLoS One*, 2016. **11**(8): p. e0160624.
35. Zatopa, A., S. Walker, and Y. Menguc, *Fully Soft 3D-Printed Electroactive Fluidic Valve for Soft Hydraulic Robots*. *Soft Robot*, 2018. **5**(3): p. 258-271.
36. Childs, E.H., et al., *Additive Assembly for PolyJet-Based Multi-Material 3D Printed Microfluidics*. *Journal of Microelectromechanical Systems*, 2020. **29**(5): p. 1094-1096.
37. Grover, W.H., et al., *Monolithic membrane valves and diaphragm pumps for practical large-scale integration into glass microfluidic devices*. *Sensors and Actuators B: Chemical*, 2003. **89**(3): p. 315-323.
38. Mosadegh, B., et al., *Next-generation integrated microfluidic circuits*. *Lab Chip*, 2011. **11**(17): p. 2813-8.
39. Weaver, J.A., et al., *Static control logic for microfluidic devices using pressure-gain valves*. *Nature Physics*, 2010. **6**(3): p. 218-223.
40. Gallardo Hevia, E., et al., *High-Gain Microfluidic Amplifiers: The Bridge between Microfluidic Controllers and Fluidic Soft Actuators*. *Advanced Intelligent Systems*, 2022. **4**(10).
41. Zhang, Q., et al., *Logic digital fluidic in miniaturized functional devices: Perspective to the next generation of microfluidic lab-on-chips*. *Electrophoresis*, 2017. **38**(7): p. 953-976.
42. Oh, K.W., et al., *Design of pressure-driven microfluidic networks using electric circuit analogy*. *Lab Chip*, 2012. **12**(3): p. 515-45.
43. Rhee, M. and M.A. Burns, *Microfluidic pneumatic logic circuits and digital pneumatic microprocessors for integrated microfluidic systems*. *Lab Chip*, 2009. **9**(21): p. 3131-43.
44. Toepke, M.W., V.V. Abhyankar, and D.J. Beebe, *Microfluidic logic gates and timers*. *Lab Chip*, 2007. **7**(11): p. 1449-53.
45. El-Atab, N., J.C. Canas, and M.M. Hussain, *Pressure-Driven Two-Input 3D Microfluidic Logic Gates*. *Adv Sci (Weinh)*, 2020. **7**(2): p. 1903027.
46. Li, D.-D., et al., *Liquid Metal-Enabled Soft Logic Devices*. *Advanced Intelligent Systems*, 2021. **3**(6).
47. Hevia, E.G., L. De La Rochefoucauld, and R.J. Wood, *Towards a Microfluidic Microcontroller Circuit Library for Soft Robots*, in *2022 International Conference on Robotics and Automation (ICRA)*. 2022. p. 7138-7144.
48. Preston, D.J., et al., *Digital logic for soft devices*. *Proc Natl Acad Sci U S A*, 2019. **116**(16): p. 7750-7759.
49. Sochol, R.D., et al., *3D printed microfluidic circuitry via multijet-based additive manufacturing*. *Lab Chip*, 2016. **16**(4): p. 668-78.
50. Song, S., S. Joshi, and J. Paik, *CMOS-Inspired Complementary Fluidic Circuits for Soft Robots*. *Adv Sci (Weinh)*, 2021. **8**(20): p. e2100924.
51. Bartlett, N.W., K.P. Becker, and R.J. Wood, *A fluidic demultiplexer for controlling large arrays of soft actuators*. *Soft Matter*, 2020. **16**(25): p. 5871-5877.
52. Wang, J. and Y. Huang, *Design and implementation of a microfluidic half adder chip based on double-stranded DNA*. *IEEE Trans Nanobioscience*, 2014. **13**(2): p. 146-51.
53. Cai, G., et al., *Variable-position centrifugal platform achieves droplet manipulation and logic circuitries on-chip*. *Lab Chip*, 2023. **23**(2): p. 349-361.
54. Zhou, Z., et al., *A Fluidic Adder Circuit Based on a Microfluidic System*. *IEEE Electron Device Letters*, 2019. **40**(6): p. 977-980.
55. Li, Z., C. Liu, and J. Sun, *Hydraulic-electric analogy for design and operation of microfluidic systems*. *Lab Chip*, 2023. **23**(15): p. 3311-3327.
56. Hubbard, J.D., et al., *Fully 3D-printed soft robots with integrated fluidic circuitry*. *Science Advances*, 2021. **7**(29): p. eabe5257.
57. Jobson, D., *On the flow of a compressible fluid through orifices*. *Proceedings of the Institution of Mechanical Engineers*, 1955. **169**(1): p. 767-776.

Acknowledgments

Funding:

National Natural Science Foundation of China grant 62205204

National Natural Science Foundation of China grant 62375172

ShanghaiTech University Startup Fund

Author contributions:

Conceptualization: WC

Methodology: YL, XZ, WC

Investigation: YL, WC

Visualization: YL

Supervision: WC

Writing—original draft: YL

Writing—review & editing: YL, WC, XZ

Competing interests: Authors declare that they have no competing interests.

Data and materials availability: All data are available in the main text or the supplementary materials.

Supplementary Materials for

3D-Printed Hydraulic Fluidic Logic Circuitry for Soft Robots

Yuxin Lin,¹ Xinyi Zhou,¹ Wenhan Cao^{1,2*}

¹School of Information Science and Technology, ShanghaiTech University, Shanghai 201210, China

²Shanghai Engineering Research Center of Energy Efficient and Custom AI IC, Shanghai 201210, China

*Corresponding author: Wenhan Cao, whcao@shanghaitech.edu.cn

Table of Content

1. Contrasting driving effects of pneumatic and hydraulic drive systems	20
2. Fluid resistance in half adder system	21
3. Basic hydraulic logic gates fabrication	23
4. Experiment of AND gate and NOT gate flow rate-control pressure testing.....	24
5. Experiment of half adder type I and type II.....	26

1. Contrasting driving effects of pneumatic and hydraulic drive systems

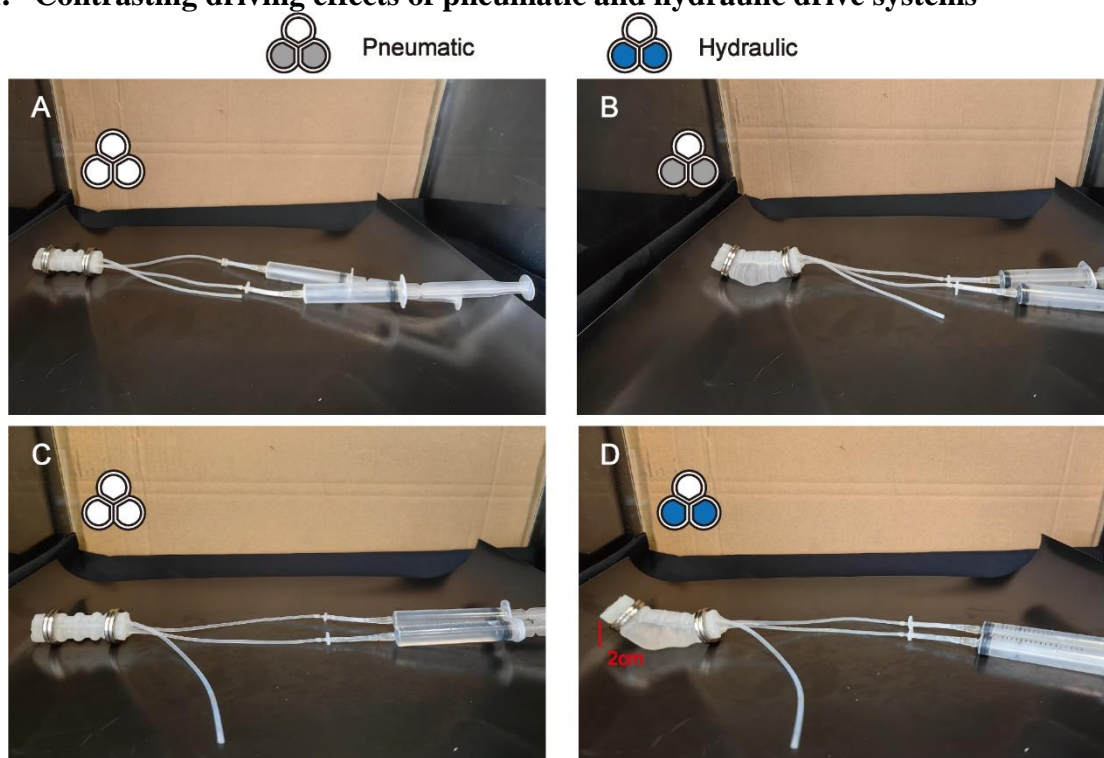


Fig. S1. Different effects produced by pneumatic and hydraulic actuation methods. The drive in (A) and (B) is pneumatic, while in (C) and (D) is hydraulic.

In order to compare the different effects produced by pneumatic and hydraulic

actuation methods, we designed the following experiment. Fix a magnet at the end of the actuator, attach it to the magnetic paper, and pass 10ml of water and air into the two chambers below the actuator to observe the deformation effect of the actuator.

Comparing the experimental results of the two Fig. S1B and Fig. S1D, we can find that when the volume of injected fluid is the same, the deformation generated by hydraulic drive is enough to lift the end of the actuator while the pneumatic drive can only cause local bending of the actuator. This is due to the compressibility of gas. Compared to gas, incompressible liquids exhibit better performance in transmitting pressure.

2. Fluid resistance in half adder system

Comparing Fig. 5F and Fig. 5I, we notice that there a significant decrease in output pressure of Carry. Since the length of silicon hose used in the experiment is the same and according to Poiseuille's law (Eq. S1):

$$R_{HOSE} = \frac{128\mu l}{\pi D^4} \quad (S1)$$

The inner diameter of the hose is 2.5 mm, and the total length of hose used to fabricating the half adder system in is 45 cm and $\mu = 0.894 \times 10^{-3}$ Pa·s when the experiment temperature is 24 °C, the total R_{HOSE} can be calculated as:

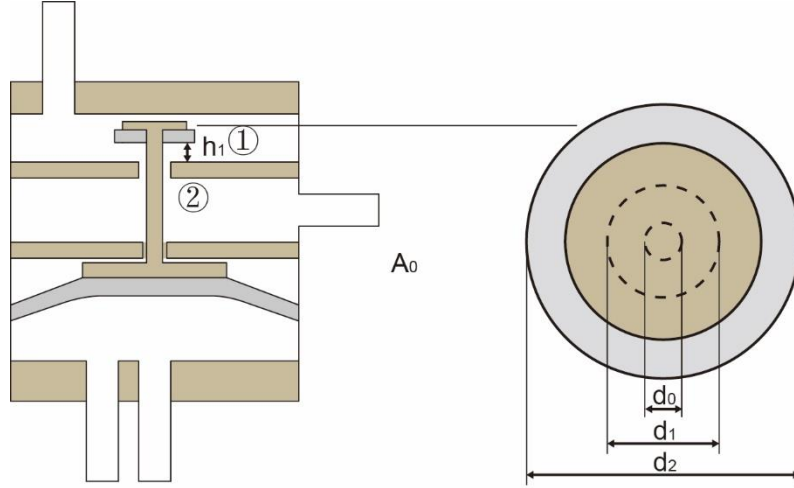
$$R_{HOSE} = 419614121 \text{ Pa} \cdot \text{s}/\text{m}^3 = 419.6 \text{ Pa} \cdot \text{s}/\text{ml} \quad (S2)$$

From Fig. 2J we know that when the input pressure is 69.28 kPa and control pressure reaches 80 kPa, the flow rate is equal to 2.5 ml/s, which leads to the pressure decreases ΔP in the hose:

$$\Delta P_{HOSE} = Q \cdot R_{HOSE} = 1.04 \text{ kPa} \quad (S3)$$

It is much small than the total pressure decrease. So the pressure drop mainly occurs inside the gate. Considering Fig .6G, there is 5 kPa decreases between Input 3 and Carry when NOT gate 3 has no control pressure, so the pressure decreases in NOT gate is 5 kPa when it is not given control pressure. In Fig. 5D there are two gates and a check valve in the circuit at work when Input 2 flows in, and the pressure decreases between Input 2 and Sum is 20 kPa Fig. 5F, so the check valve is responsible for the 10 kPa decreases.

However there is no check valve in circuit at work in Fig. 5G, and total pressure decreases reaches nearly 70 kPa. The structure of AND gate is the primary factor causing pressure drop.



d_0 : diameter of pole

d_2 : diameter of carrier ring

d_1 : diameter of orifice

h_1 : height of plate gap

① fluid resistance of flat plate gap

② fluid resistance of thin-wall orifice

Fig. S2 The flow resistance caused by AND gate structure.

As shown in Fig. S2, significant flow resistance is potentially caused by two specific regions. First region is caused by limit of the rising height of disc-pole-disc structure. The maximum of $h_1 = 0.9$ mm, $d_0 = 1$ mm, $d_1 = 3$ mm and $d_2 = 5$ mm according to the formula of fluid resistant of flat plate gap flow (Eq. S4):

$$R_{PLATE} = \frac{12\mu(d_2 - d_1)/2}{\pi \frac{(d_1 + d_2)}{2} h_1^3} \quad (S4)$$

R_{PLATE} is calculated as $R_{PLATE} = 1561421.3 \text{ Pa} \cdot \text{s/m}^3 = 1.56 \text{ Pa} \cdot \text{s/ml}$. This resistance is small so it is not the main factor. The thin-wall orifice plays an important role in fluid resistance. According to the orifice flow formula:

$$Q = C_q A \sqrt{\frac{2\Delta p}{\rho}} \quad (S5)$$

By performing variations, we could obtain formula of fluid resistance for thin-wall orifice flow (Eq. S6):

$$R_{ORIFICE} = \frac{\sqrt{\Delta P \rho}}{C_q A} \quad (S6)$$

In this formula the ΔP is pressure decrease, ρ is the density of the fluid, A is the cross-sectional area and C_q is an empirical constant, which falls within the range of 0.6 to 0.9. It shows that the flow resistance is related to pressure drop. In this experiment, the

$R_{ORIFICE} = \frac{\Delta P}{Q} \approx 3.2 \times 10^{10} \text{ Pa} \cdot \text{s/m}^3$, which is larger than the value

$1.56 \times 10^9 \text{ Pa} \cdot \text{s/m}^3$, obtained from the formula. It is explainable that as the cross section is an annulus so the formula needs to be some modified.

3. Basic hydraulic logic gates fabrication

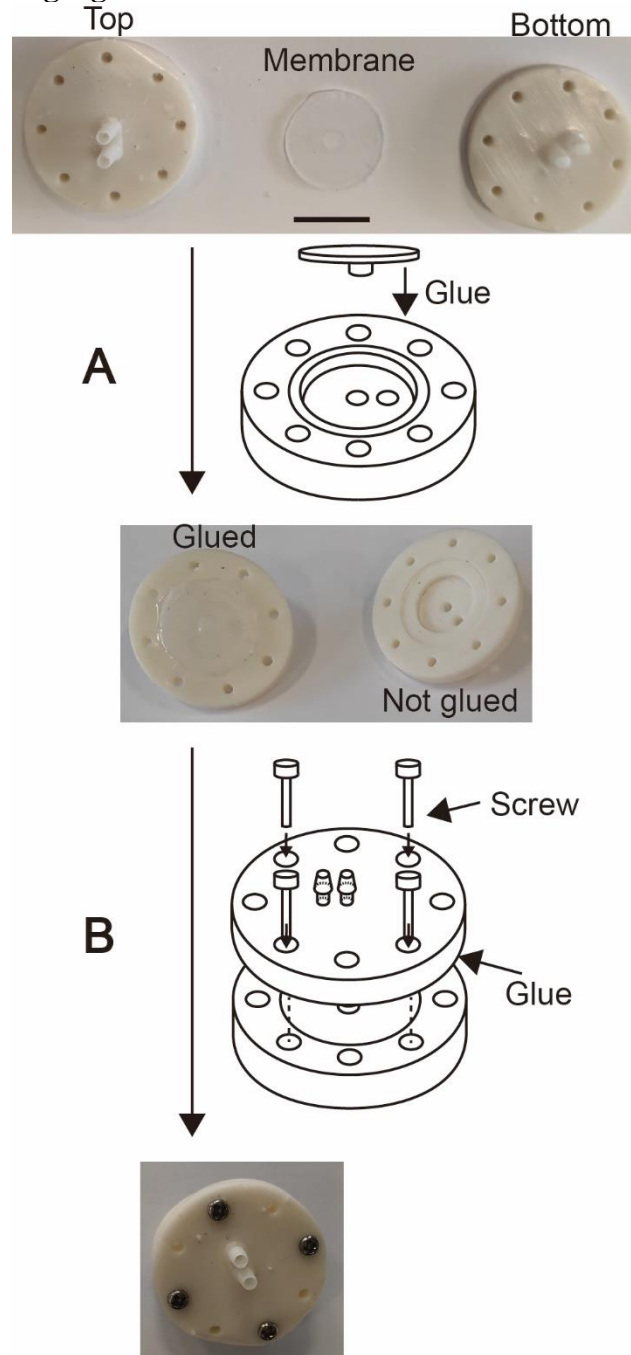


Fig. S3. Assembling procedure of NOT gate. In procedure A using glue to stick the membrane onto the upper shell. In procedure B using glue to stick other side of membrane onto the bottom shell and fastening the four surrounding bolts to secure the upper and lower shell casing together.

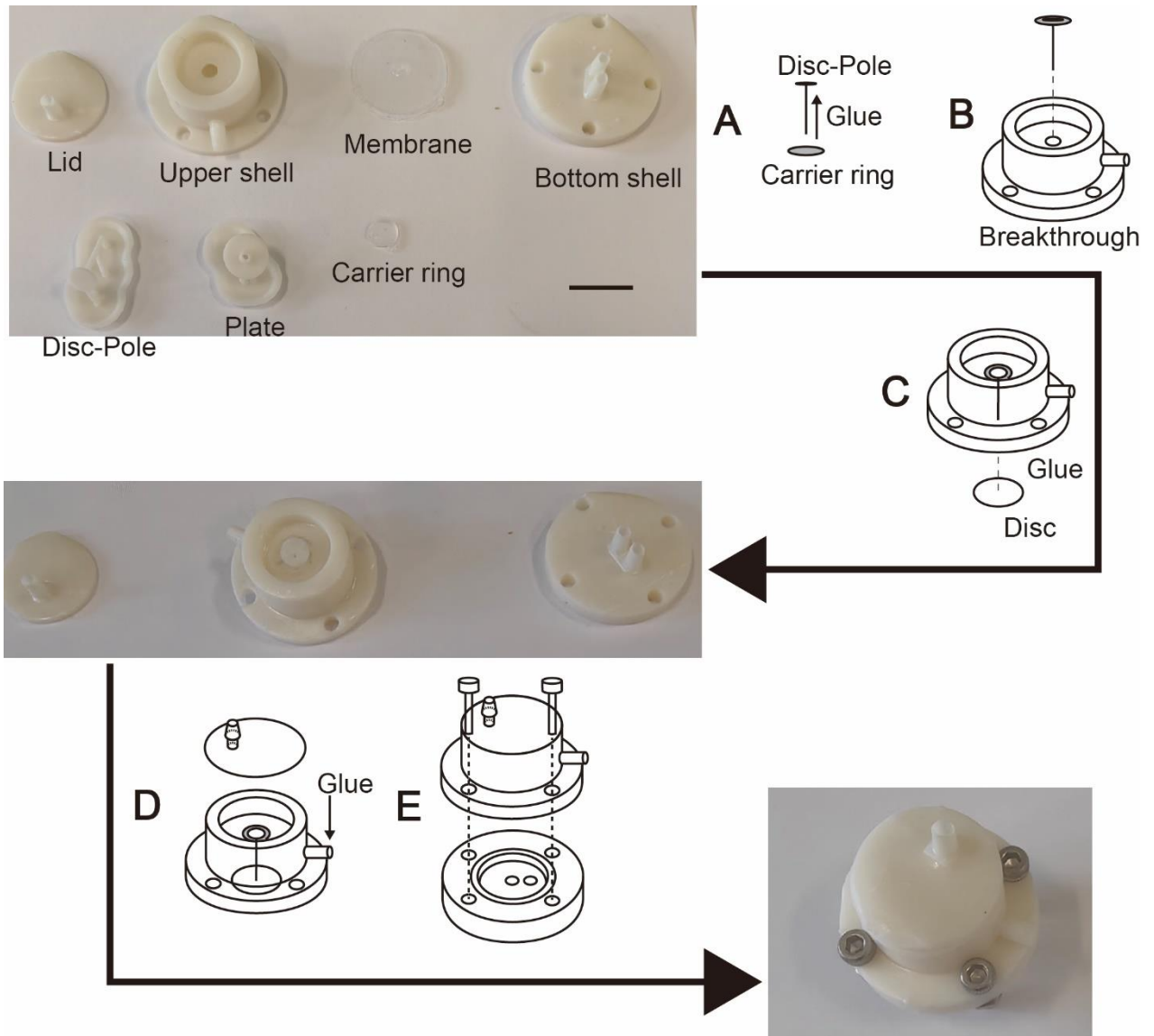


Fig. S4. Assembling procedure of AND gate. In procedure A, using glue to stick the carrier ring to the underside of the pole top. In procedure B threading the entire pole through the upper shell. In procedure C using glue to stick the plate onto the bottom of the pole. In procedure D using glue to stick the lid onto the upper shell. In procedure E fastening the four surrounding bolts to secure the upper and lower shell casing together.

4. Experiment of AND gate and NOT gate flow rate-control pressure testing

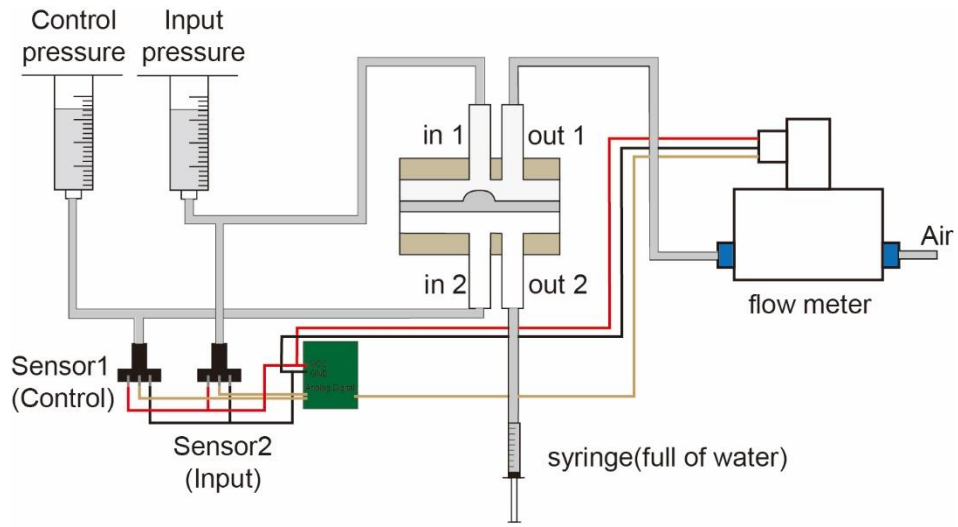


Fig. S5 wiring diagram of the NOT gate testing.

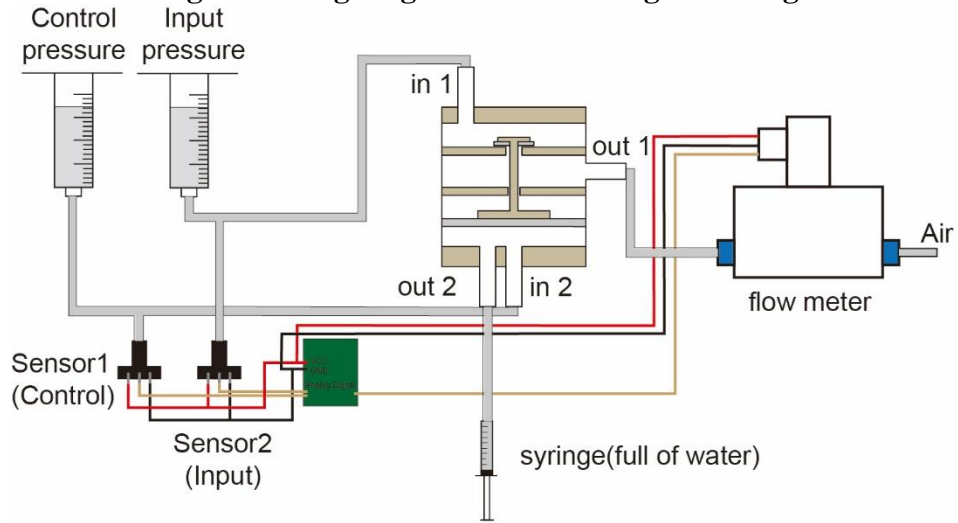


Fig. S6 wiring diagram of the AND gate testing.

5. Experiment of half adder type I and type II

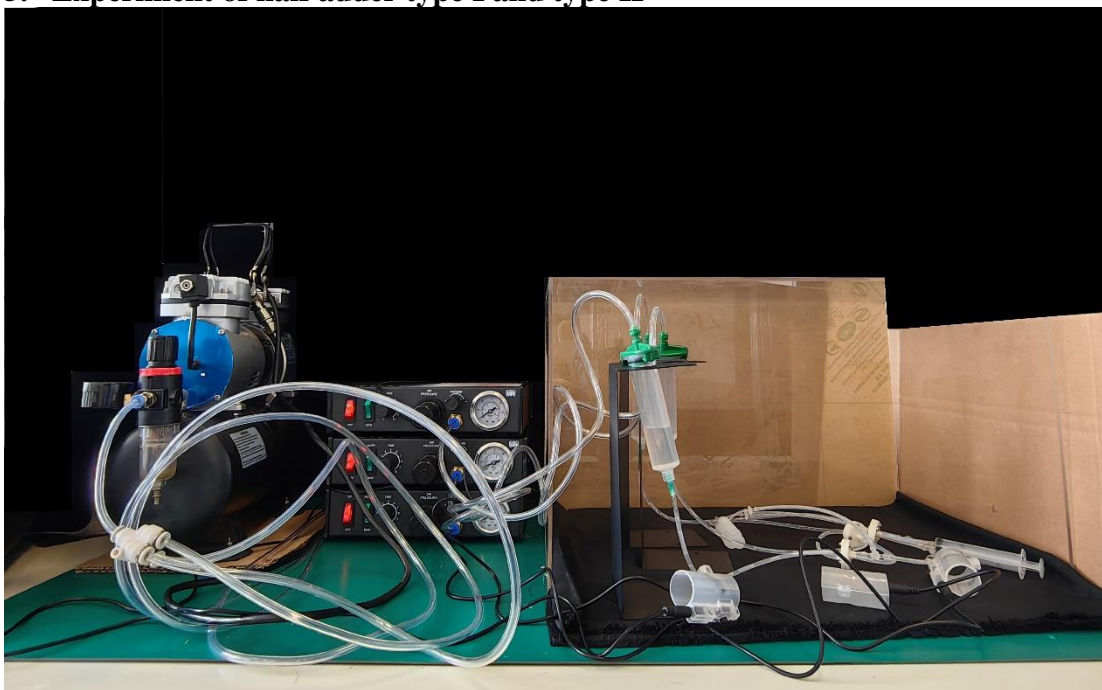


Fig. S7 Experimental device.